

High Precision Figure Verification of a Lightweight UV Mirror

PIP II Report

Scott Antonille

Code 551, Optics Branch
NASA / GSFC

Mentors: Mark Wilson David Content
Code 551, Optics Branch Code 551, Optics Branch

SHARPI PI: Doug Rabin
Code 682, Solar Physics Branch

Abstract

A background and test plan for the surface figure verification of a large aperture lightweight UV mirror is presented. The task is to develop the means to successfully verify that the Kodak FUV lightweight 50cm CA f/1.3 parabolic mirror meets the 6.3nm RMS surface figure specification upon its imminent delivery. At the time of writing, the mirror has not been received. However, initial tests limit the uncertainty introduced by the test optics into the surface figure error measurement to less than 0.008wvs RMS at spatial frequencies between 1.5mm and 30mm over the radial region 70mm-100mm. We expect more accurate test setups to reduce this uncertainty. Our goal is to reduce the final uncertainty in the surface figure measurement to 3.15nm or $\lambda/200$. Additionally, software has been developed which will enable the measurement, mapping, and subtraction of error upon further test setup refinement.

1 Introduction

My effort during my PIP II has fallen under two major tasks: Lightweight Optics Internal Research and Development (LWIR&D), and the development of the Solar High Angular Resolution Photometric Imager (SHARPI) telescope. LWIR&D is tasked with developing the facilities and expertise necessary to qualify large-aperture, smooth, ultra-precise lightweight optics. The Optics Branch at NASA Goddard is scheduled to receive such a mirror from Kodak: a 20inch f/1.3 parabola with an areal density of $19.75kg/m^2$ and a 6.3nm RMS surface figure error¹ specification. The SHARPI telescope would require a mirror of this size and quality to achieve its intended goal of 0.2arcsec solar imaging at 160nm, a state of the art solar resolution at that wavelength (see Table 1). My effort has concentrated on making an in-house verification of this ultra-precise surface figure specification possible.

Mission	Quoted Resolution <i>arcsec</i>	At Closest λ to 160nm <i>nm</i>
SOHO/EIT	2.6	30
TRACE	1	160
SERTS	1	30
Non-Solar Imaging Missions		
Galex	3.3	160
FUSE	1.5	120
Proposed Missions		
Solar-B/SOT	0.5	480
SHARPI	0.2	150

Table 1: Other UV Missions

Fabrication and verification of high precision mirrors, especially mirrors used in the ultraviolet, requires high precision surface figure metrology. High precision surface figure is of greater importance as the wavelength of interest shortens. A mirror whose imaging ability is limited only by diffraction at optical wavelengths² quickly becomes limited by its surface figure error in the UV³. A standard criteria for diffraction limited optics is that the surface

¹Conventionally, surface figure error has a spatial frequency greater than $0.01mm^{-1}$. However, interferometers can measure errors with higher spatial frequencies.

²400nm-780nm

³Ultraviolet, 10nm-400nm

figure error cannot exceed $\lambda/28$ RMS. At optical wavelengths, this translates to approximately 20nm RMS; at a UV wavelength of 160nm, however, the criteria is 6nm RMS, assuming a perfect optical alignment. Surface figure metrology is conventionally done with phase shifting interferometry at the HeNe laser wavelength of 632.8nm. Therefore, to test the 6nm RMS criteria with a HeNe laser requires a wavefront accuracy and precision exceeding $\lambda/100$. At present, this lies in the domain of high precision surface figure metrology.

High resolution UV imaging not only demands a high precision mirror but also a large aperture. Once diffraction limited, the resolving power of a telescope is directly proportional to λ/D , where λ is the wavelength and D is the diameter of the primary optic. However, simply scaling the mirror upwards increases the mass of the mirror drastically, making the delivery of these telescopes to orbit—above the UV obscuring atmosphere—costly and difficult. If the mirror is lightweighted, a larger diameter mirror can be launched with a mass much less than traditional mirrors. Since this is paramount to both Earth and Space Science, many lightweighting schemes are under development, in test, or in use.

The f/1.3 annular parabola to be delivered by Kodak has a 508mm clear aperture and 140mm inner diameter⁴ but weighs only 4.5kg (Table 2). This glass mirror consists a thin faceplate and backplate fused to a water-jet cut honeycomb core. The mirror is then lapped and ion-figured to the surface specifications in Table 3. Table 4 compares the Kodak mirror to several other mirrors of comparable surface figure, diameter, or areal density. The combination of high precision surface figure, aperture, and areal density make this mirror both unique and state of the art. Because of its unique and demanding specifications, it will be a challenging task to verify that this mirror meets its surface figure specification of 6.3nm RMS.

2 Surface Figure Verification Test Plan

2.1 Concept

There are three main methods commonly applied to perform global surface figure metrology on a parabola: an auto-collimated double-pass test, a retro-ball test, and a null lens test. To perform a double-pass test, a spherical

⁴The mirror is 55cm full aperture, but it was infeasible to bring the mirror within specifications over the entire aperture.

⁵By Kodak's calculation

⁶Without spherical aberration

Material	Fused Silica	
Outer Diameter	558	mm
Clear Aperture	508	mm
Inner Diameter	139.7	mm
Edge Thickness	48.26	mm
Mass	4.54	kg
Areal Density	19.75	kg/m²
Lightweighting	81.52%⁵	

Table 2: Lightweight Kodak UV Mirror, Physical Properties

Radius of Curvature at Vertex	1292.6	mm
Conic	-1	
Global Surface Figure Error (>10mm)	6.3	nm RMS
Mid-Frequency Surface Figure Error (1mm-10mm)	2.5	nm RMS
Microroughness (1μm-1mm)	1.0	nm RMS

Table 3: Lightweight Kodak UV Mirror, Surface Specifications

	<i>notes</i>	Areal Density <i>kg/m²</i>	Surface Figure Error RMS <i>nm</i>	Diameter of Optic <i>cm</i>	Intended Band
HST		180	6.3 ⁶	240	UV, VIS
JWST – Goal		15			IR, VIS
SIRTF	Beryllium	28	67	85	IR
SBMD – Ball Aerospace	LW Beryllium	9.8	19	53	
SLMS – Shafer	Foam Core	9.8	17	10.5	UV
FIRST (Herschel) Demonstrator Mirror	SiC based	26	1310	135	IR
Prop. SHARPI PM – Kodak	Fused Silica – Honeycomb Core	20	6.3	50.8	UV
FUSE	OAP - unmounted	54	16	37	UV

Table 4: Comparable Lightweight Mirrors

wavefront is centered at the focus of the parabola, which is then collimated by the mirror. The collimated beam is then retro-reflected by a flat, thereby returning to the parabola and refocusing at the

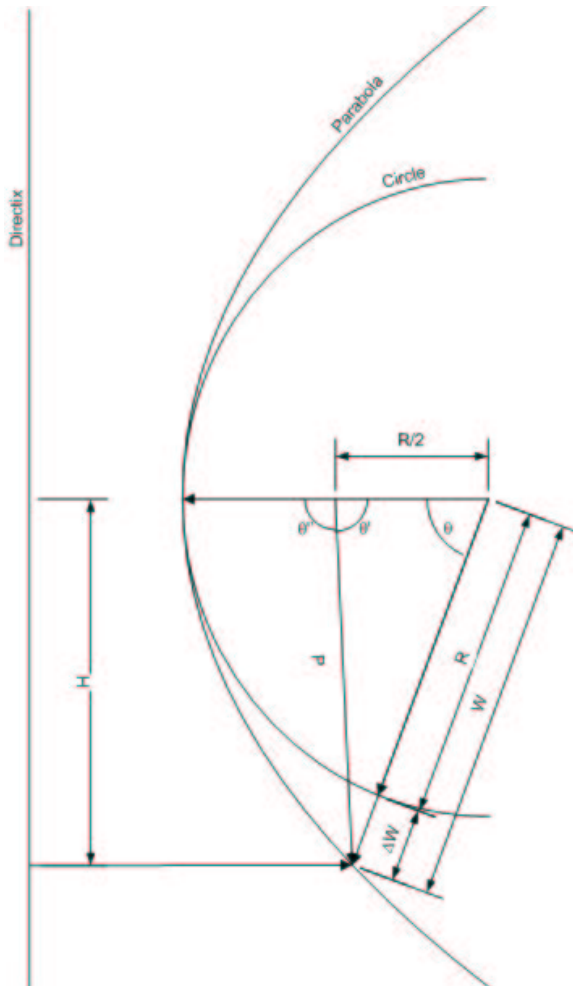


Figure 1: Finding ΔW .

of the wavefront. The departure from a perfect spherical wavefront at the focus then represents the departure of the parabola and flat from their ideal shape. To determine the surface figure error of the parabola to an accuracy of less than $\lambda/200$ RMS, the reference flat cannot induce an uncertainty of greater magnitude. Traditionally, this has meant that the flat's surface error could not be greater than $\lambda/200$ RMS or some fraction thereof. With higher resolution digital interferometers, a technique of mapping the surface figure error of the reference flat and then subtracting from the final wavefront is possible. The uncertainty in this subtraction still cannot exceed some fraction of $\lambda/200$. Unfortunately, a 50.8cm flat was not available, and moreover, a precision calibration of a 50cm flat to an uncertainty of less than $\lambda/200$ was not feasible. However, *the technique of subtracting an optic's aberration contribution to wavefront is a useful concept and will be employed in tests where test optics can be precision tested.*

The retro-ball test requires the generation of a collimated beam matching the size of the test optic. The parabola focuses the collimated beam onto a spherical reflective ball bearing centered at the focus. The ball reflects

the light back to the parabola where it is re-collimated and returned to the interferometer. By rotating the ball and averaging results, the uncertainty that originates from the surface error of the sphere is minimized.⁷ Although this source of uncertainty is minimized, the test still requires generating a large collimated beam from an interferometer whose wavefront accuracy is comparable to the $\lambda/200$ specification. We do not have access to such a system, and a $\lambda/200$ RMS wavefront accuracy is difficult to achieve with a 50cm collimated beam. Calibration or acquisition of such an instrument is not within the scope of this task; however, if the use of such a system might become available, we would consider this a potential test.

The null lens test⁸ is a center of curvature test. Specifically, the null lens aberrates the input beam so that the foci of the mirror surface become co-located. In order for this to work, the null lens needs to aberrate the input wavefront by twice the amount that the surface deviates from a sphere. In figure 1, this wavefront error is $2\Delta W(\theta)$. Defining $\theta'' = \pi - \theta'$, using the law of cosines, and manipulating the polar equation of a parabola, I find that:

$$W(\theta'') = R\sqrt{\left(\frac{1}{1 + \cos\theta''} + \cos(\theta'')\right)^2 + \frac{1}{2}\sin^2\theta''} \quad (1)$$

$\Delta W(\theta'')$ is then simply $W(\theta'') - R$. To analyze ΔW over an optic of a particular $f/\#$, θ'' runs from 0 to θ''_{max} which is:

$$\theta''_{max} = 2 \tan^{-1}\left(\frac{1}{4 f/\#}\right) \quad (2)$$

To transform $\theta'' \rightarrow \theta$, use the equation:

$$\theta = \sin^{-1} \frac{R \sin \theta''}{W(\theta'')(1 + \cos \theta'')} \quad (3)$$

Figure 2 shows ΔW over the diameter of our $f/1.3$ $R = 1292.606mm$ parabola. A common means of describing wavefront error is by Zernike polynomials. Because ΔW is only a function of the radial distance on the mirror, the angularly dependent Zernikes terms will not contribute. Therefore, to derive the wavefront error required to do a null lens test on our parabola, only the radial Zernike terms are pertinent. The first two radial Zernike terms are insignificant as they represent piston (a constant) and focus (which can be physically removed by refocusing). We are, however,

⁷As long as the ball is and stays properly centered.

⁸Or, similarly, any means of generating a parabolic wavefront

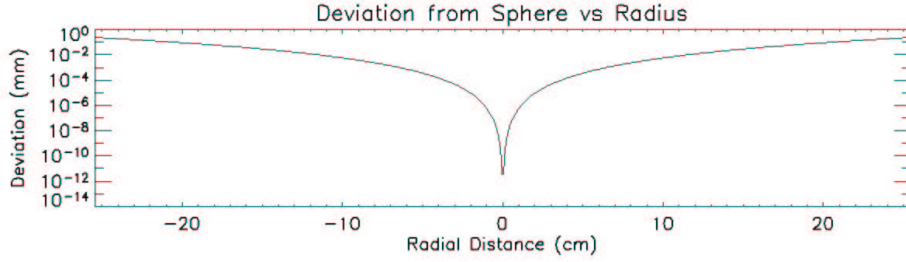


Figure 2: Deviation of a f/1.3 1292.6mm radius parabola from a circle of equal radius. The deviation is the distance between the parabola and circle along a line projected from the center of the circle. Deviation is plotted as a function of aperture height.

nm	mm	wvs @ 633nm	Term
163267	0.1633	258.0	Focus
86702.1	0.0867	137.0	3 rd Order Spherical Aberration
5.35583	5.4E-06	0.0085	5 th Order Spherical Aberration
0.80646		0.0013	7 th Order Spherical Aberration
0.00013		2.1E-07	9 th Order Spherical Aberration
0.00001		1.9E-08	11 th Order Spherical Aberration

Table 5: The RMS contribution of various Zernike terms to the total Zernike fit on the of the parabola-sphere deviation.

focused on the various orders of spherical aberration. Here, they are listed as radial Zernike terms 2 and higher. The transformation of this difference into the radial Zernike polynomial set generates a infinite but convergent set of Zernike coefficients. Figure 3 plots the various values of these terms as a function of term number. Because our desired accuracy is on the nanometer scale, the 5th and higher terms can be ignored, as they contribute an insignificant amount. Therefore, the Zernike terms that will be relevant are the 3rd, 5th, and 7th order spherical aberration. Table 5 shows the various root mean squared (RMS) contributions from these Zernike terms over the entire 2-D un-obscured f/1.3 parabola.

A refractive compound cemented null lens design was not found. Airspaced compound lenses we undesirable because of alignment difficulties. The difficulty is that we have an enormous amount of 3rd order spherical aberration, leading to a complex null lens design. Additionally if an extreme or ultra-precise lens is required, the lens would then have to be tested

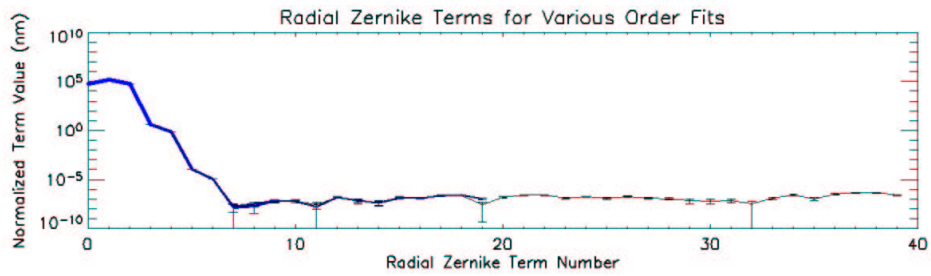


Figure 3: Magnitude of the normalized radial zernike coefficients (*in nm*) as a function of term number for the fit to the difference between a $f/1.3$, $20in$ clear aperture parabola and a sphere of identical vertex curvature. The term number is plotted along the x -axis and the normalized radial Zernike term is plotted on the y -axis. Fits of various order are over-plotted: 40th order, 20th order, 10th order, 6th order, and 4th order. The lowest order fit is represented by the thick blue line, and the highest order fit is represented by the thin black line. It is apparent that the overlapping terms are consistent over various order fits. For this parabola, the fifth and higher terms contribute an insignificant amount compared to the desired accuracy of our test. This corresponds to ninth order spherical aberration and higher. Therefore, a null lens in this application must correct for 3rd-7th order spherical aberration to within several nanometers.

– leading to another difficult test.

However, because we are testing at the HeNe laser wavelength, we can utilize a diffractive lens called a computer generated hologram (CGH). A diffractive lens is a hologram created by etching a diffractive screen from a substrate. The frequency of this screen is such that the first order diffraction of the test beam through the screen creates the desired wavefront. In this case, the frequency of the hologram is a function of radial distance from the center, and creates the wavefront distortion equal to $2\Delta W$. With the CGH, it is possible to impart these extremely large spherical aberration terms into the wavefront. However, CGH's have not traditionally been used to the $\lambda/200$ RMS accuracy we require. In fact, the manufacture's tolerances on a typical test setup contribute to a $\frac{7}{100}\lambda$ RMS surface figure error. The intrinsic accuracy of the CGH, however, is not overwhelming. The stated tolerances on the fabrication of the CGH are $\frac{1.8}{100}\lambda$, and these tolerances include several factors which can be accounted for. Clearly the CGH must be qualified; however, the CGH test does offer us the ability to test an f/1.3 50.8cm parabola to our approximate accuracy with a minimum of cost. To reach our desired accuracy, though, we must model, compensate for, and subtract systematic errors.

2.2 Figure Verification Test Setup

Shown in Figure 5, the CGH Figure test involves four major optical components: the interferometer, the transmission sphere, the CGH, and the parabolic test piece. The interferometer is a MARK IV/GPI interferometer. The transmission sphere takes the input beam and converts it to a converging f/1.5 beam. 90mm in front of that focus, the CGH intercepts the converging beam and imparts its characteristic aberration. The beam then propagates to the mirror where it is retro-reflected back through the CGH and the transmission sphere into the interferometer where the wavefront is measured through phase shifting interferometry.

Currently, we do not have possession of the mirror. We are, however, developing and fabricating the exact metrology fixtures. The emphasis of the PIP II period was on qualifying the test optics involved in this test, as well as developing the means to measure and account for them.

2.3 Test Flow

In order to successfully verify that the Kodak f/1.3 parabolic mirror meets its 6nm RMS surface figure specification in a 0g environment, no test optic

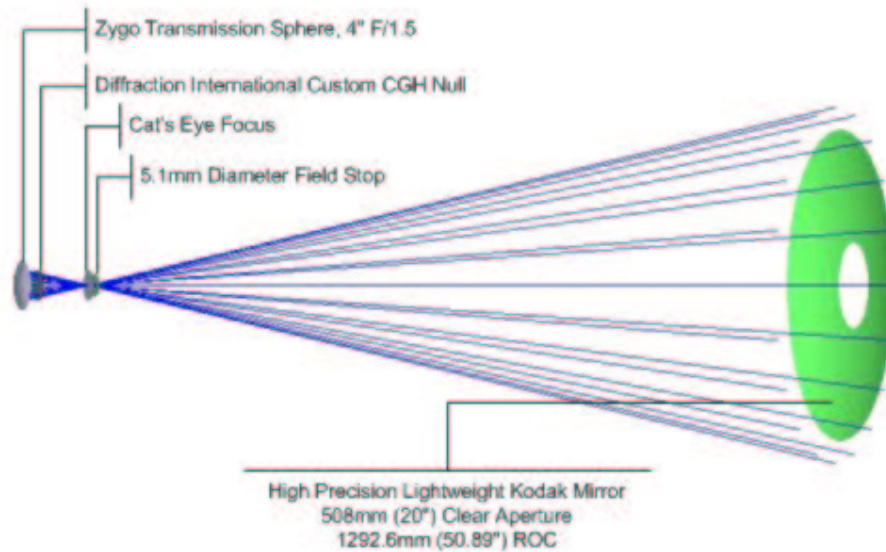


Figure 4: CGH Figure Test Setup

or model can introduce an error to the final surface figure error calculation that would make the verification impossible. This includes the CGH, the transmission sphere, and the 1g surface sag model that must be subtracted from the measured surface figure error to yield the 0g surface figure error. We do not require that each of these elements contribute less than a total of $\lambda/200$ error. Rather, we intend to measure and subtract the error that these elements imparts. Therefore, it is the uncertainty in the subtraction which must not accumulate to more than a $\lambda/200$ error in the final result.

It is necessary to test each element in some way. Where other optics or models are used to test these elements, those elements themselves must be tested. Figure 5 shows the current test plan to accomplish the desired certainty. This is a recursive process. Test setups have been improved, optics have been refigured, and analyses been refined. All tests have been and will be repeated until the desired accuracy has been met.

2.3.1 1g Sag Table

The mirror has been fabricated so that it has its correct figure while experiencing no gravitational load. However, we must test it in 1g.

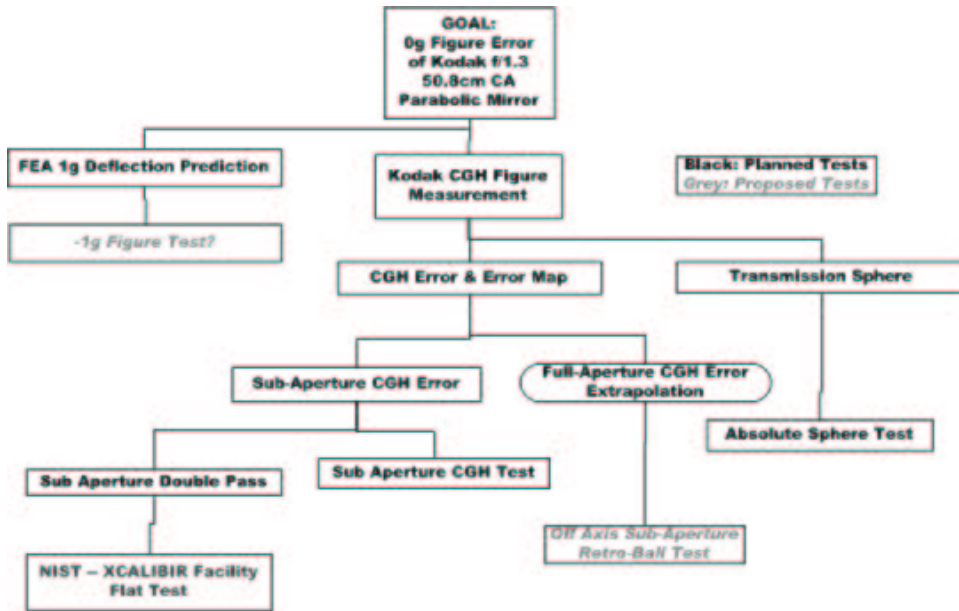


Figure 5: Test Plan Flow

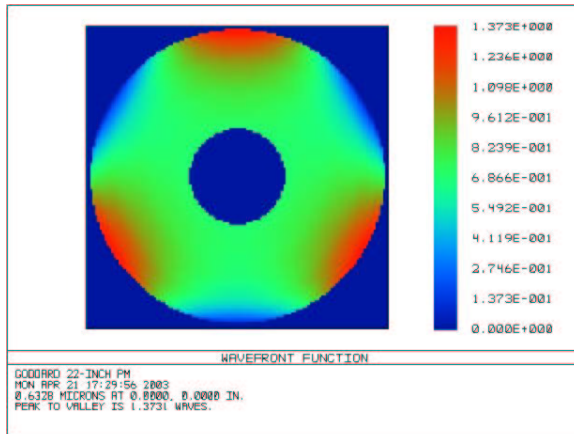


Figure 6: Wavefront aberration in the surface figure test resulting from the 1g surface sag.

This leaves us with the problem of anticipating the surface sag and subtracting it from the final measured result. Kodak’s FEM was analyzed by Sandra Irish, Code 542 – Mechanical Analysis and Simulation Branch. These results were interpolated over a regular grid and converted into a Zemax grid sag surface. Figure 6 shows the expected wavefront distortion caused by the 1g sag— a RMS wavefront error of 0.2 waves or approximately 127nm.

The vendor's standard allocation for the model's uncertainty is 5%, or here a $\lambda/200$ uncertainty in the measurement of our figure error. This alone is the desired uncertainty of our entire test. It is necessary to reduce this uncertainty in some way. One proposed solution is to reverse the orientation of the test mirror, so that it experiences a -1g load. In this case, the +1g and -1g figure errors could be averaged to produce a check of the sag model.

2.3.2 Transmission Sphere

The transmission sphere is one of the primary elements of the CGH figure verification test. In order to measure its contribution to the measured error, the "absolute sphere test" is employed. The transmission sphere is tested against a concave spherical mirror in three configurations. Using a linear combination of these tests, it is possible to isolate the contribution of each optic to the final measured wavefront. Because this measurement isolates the contribution of each optic, it is considered an "absolute" test.⁹

The initial results were that the reference wavefront generated by the transmission sphere had a wavefront aberration of 0.004wvs (2.5nm) RMS \pm 0.0018wvs (1.1nm).¹⁰ This accuracy and precision are on the order required. Additionally, the concave reference sphere used in this test was precision calibrated by the Zygo Corporation to an estimated accuracy of 0.001wvs. Their result for the RMS surface error of the sphere in our region of interest is 0.006wvs RMS. This compares well with our measured RMS surface error of 0.005wvs \pm 0.0018wvs.

The final uncertainty introduced by the transmission sphere plus the uncertainty from the CGH and remaining figure components must not exceed $\lambda/200$. The error introduced by the transmission sphere approximately meets our final specification. Although presently leaving no room for other sources of uncertainty, it will be put in the background until the other contributions to our test error have been reduced to a comparable level. At that point, this test will be repeated with a much more rigorous and precise test setup. With this information, the affect of the transmission sphere will be subtracted from our final result.

⁹For more details on this test, see appendix, or see the notes from the 22 April, 2003 presentation, "High Precision Figure Verification of a Lightweight UV Mirror."

¹⁰There is some discussion to whether the results can be trusted to this precision because of potential internal retrace errors.

2.3.3 Computer Generated Hologram

Qualifying the CGH is the most challenging aspect of the test plan because it imparts such a large amount of spherical aberration. Our initial plan was to fabricate an independently verifiable smaller optic to take the place of the 50cm parabola. Unfortunately, because of the enormous amount of spherical aberration in the wavefront, there is no easily tested optic that compensates for the spherical aberration and retro-reflects while capturing the entire beam. Instead, we chose to test a sub-aperture of the Kodak mirror. A 9.5" diameter parabola with the identical vertex radius was fabricated and used to mock up the central region of the full aperture Kodak mirror. The sub-aperture can then be independently tested in an auto-collimating double pass test, and the results can be compared to a CGH test of the same piece.

The sub-aperture piece was fabricated with a diamond turning machine. The error in the initial fabrication was over $\lambda/2$ RMS. This would not be acceptable for a comparison between the two tests because the error in the sub-aperture mirror would far exceed any difference between the double-pass test and the CGH test. By compensating for the systematic radial diamond turning errors, the radially symmetric error was reduced to 0.15wvs RMS. Although this is not on the order of the required accuracy of the final test, the measurements are more easily compared between the CGH and double-pass test. Additional sub-aperture corrective cutting is planned to further improve its figure.

Another consideration in this comparison between the double pass test and the CGH test is the wavefront error contribution of the flat mirror to the double pass measurement. A test of the flat shows that the surface error over the 9.5" diameter is approximately 0.03wvs RMS. This was not a concern in the initial tests when a gross comparison was desired. In fact, it's the contribution to the error in the double pass test is diminished for two reasons: for one, the error is concentrated in the outer edge of the flat, where there also is a good deal of dropout on the parabola, and secondly, the flat only causes one reflection while the parabola reflects twice — and this means the uncertainty in the flat is weighted by half. This error can be taken into account, however, when it becomes important. In fact, the mirror will be precision calibrated at NIST's XCALIBIR facility to a pixel-to-pixel accuracy of 0.001wvs RMS. With proper fiducials known and aligned, the flat's contribution to the final error can be subtracted and eliminated to a degree that exceeds our required certainty.

The obvious downfall is that the outer annulus of the CGH corresponding to the radial zone on the mirror between 4.75" and 10" is not qualified. In

addition, this is where the largest wavefront distortion must take place. By determining the departure between the two independent measurements as a function of radius, we could conceivably do an extrapolation to the rest of the CGH. However, that extrapolation would come with uncertainty. I have proposed, therefore, that an off-axis portion in the outer annulus of the Kodak mirror be available to test in a retro-ball setup while the entire aperture is under test with the CGH. This would give us further insight into the behavior of the CGH at the edge of the 50cm aperture.

3 Preliminary CGH Qualification Results

3.1 Double Pass Results

Measuring the sub-aperture parabola in the auto-collimating double-pass setup had two purposes: to measure the radial error so that I could generate a new compensating corrective cut profile for the diamond turning machine and to characterize the surface figure error of the mirror to compare with the results generated in the CGH test. For the corrective cut, we are only interested in radial error only—that is, error that is only dependent on the radius ρ as measured from the center of the piece, and not error that is dependent on the angle θ to any particular point on the mirror. Because diamond turning has an inherent radial symmetry, we expect to see the radial error dominate.

Radially asymmetric errors could come from fabrication or alignment of the test setup. Radially asymmetric fabrication errors would come from a deviation in the diamond turning machine’s symmetry which would have a periodic dependence on θ — such as a wobble of the mirror on the spindle of the diamond turning machine. If reasonable attention is paid to setup and execution of the cut, this θ dependent error is minimal compared to the amount of radial error. Alignment errors, on the other hand, contribute heavily to the θ dependent error.

The equipment used in these tests was not stable and repeatable enough to minimize these radially asymmetric errors to within $\lambda/10$. A tolerance analysis showed that this radially asymmetric error would be concentrated in Zernike terms corresponding to 3rd order coma and astigmatism. These are low spatial frequency errors; that is, the period of the errors are approximately equal to some large fraction of the optic’s diameter. In the initial absence of better alignment tools, the low spatial frequency radially asymmetric errors were removed for both the generation of the compensating corrective cut and the comparison between the CGH and the double-pass

tests.

For both the corrective cut and the comparison between the CGH and double-pass tests, we are interested in the error as a function of radius. Therefore, we need to transform the cartesian coordinates of the CCD pixels to the polar coordinates of the mirror. This requires knowledge of where the center of the piece is. Luckily, the diamond turning error marks can serve as our guide, as they are almost perfectly symmetric about the center of the mirror. To make the transformation, I first did a 2-D low order Zernike fit to the data. (Figure 7(a),6(b)) For this fit, a reasonable approximation of the center is used; the residual is then examined. (Figure 7(c)) A first guess coordinate is picked as the center, and the coordinates are transformed into polar coordinates. Each x, y point now has a ρ, θ associated with it. The mean and standard deviation are then calculated for 0.1mm segments over $\rho = [0, \rho]$ for all θ . The root sum square of these standard deviations is calculated and minimized as a function of the x, y coordinate of the center. The final projection of the residual into radial coordinates can be seen in Figure 8(a). The spherical aberration associated with the 2-D fit (Figure 8(b)) and the residual are then combined to create a total radial profile(Figure 8(c)).

To generate the corrective cut, the radial profile is fit to radial Zernike terms. The radial Zernike terms correspond to the Legendre polynomials as a function of $2\rho^2 - 1$. An appropriate maximum order must be picked so that the the error of the mirror exceeds the RMS residual to the radial Zernike fit by several orders of magnitude. For the corrective cut, the Legendre polynomial is re-sampled over the desired coordinates of the cut.¹¹

The RMS of the total two dimensional measured phase is 0.25wvs while the radial contribution to this is 0.15wvs. The magnitude of the remaining radially asymmetric error is in agreement with what was expected from the current alignment tolerances of the double-pass test.

3.2 CGH Sub-Aperture Test Results

Many of the methods used to analyze the double pass measurements are re-applied to the CGH sub-aperture test. Modeling the current alignment tolerances showed the misalignment will show up as low order radially asymmetric error. Therefore, the same analysis techniques used on the sub-aperture double pass data are utilized here to minimize the contribution of the θ -dependent error introduced due to misalignment.

¹¹More details on the corrective cutting process will be reviewed in a future memo once we have exhausted the improvements of corrective cutting.

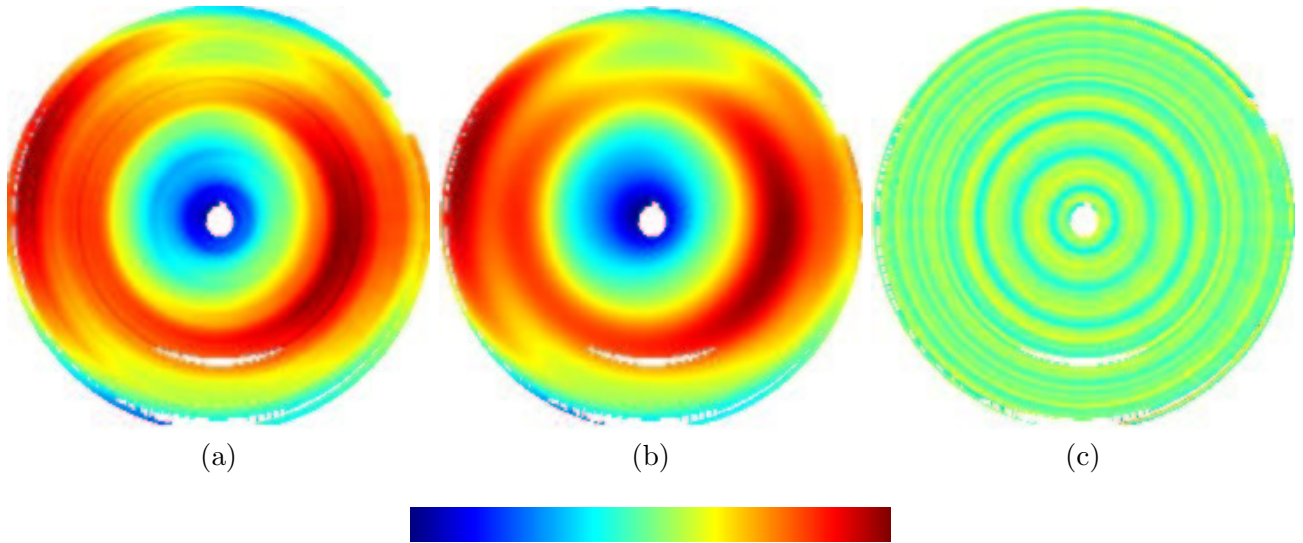


Figure 7: *Left to Right:* (a) Measured phase, (b) 2-D Zernike Fit, and (c) Residual to the fit, for the current sub-aperture diamond turned parabola via the double pass test. The scale, at bottom, runs from 0wvs (at 632.8nm) to 1.3wvs.

White indicates no data.

Figure 9(a) shows the measured phase from the CGH sub-aperture test. The three major contributions to the error are 3^{rd} order coma, 3^{rd} order astigmatism, and radial symmetric error. As in the double pass analysis, the radially symmetric error is extracted (Figure 9(b)) and analyzed. With that data, a radial profile is extracted (Figure 10).

3.3 Agreement of Tests

To compare these two results, it is first useful to compare what has been removed from each measurement to make the comparison. Figure 11 shows the θ -dependent error which has been removed for comparison. These terms most likely result from misalignments in the test setups. For the double pass setup, the main term which has been removed is astigmatism. The source of this astigmatism from the double-pass auto-collimating setup is most likely a boresight error. From the CGH measurement, both astigmatism and coma have been removed. The most likely source of this error is the alignment of the CGH. Micron decenters and arcminute tilts can create astigmatism and

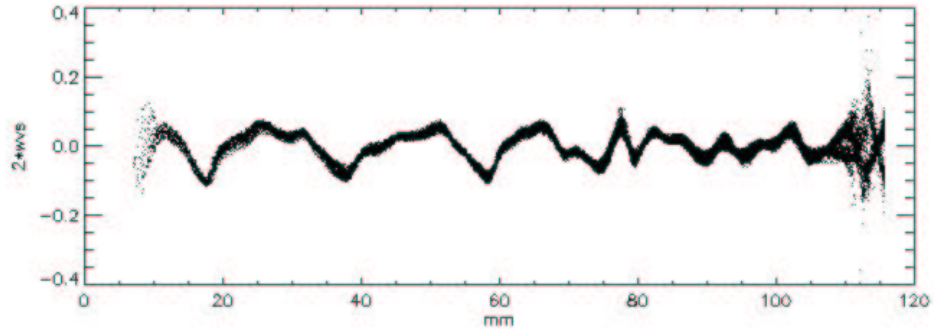
coma of this magnitude. It is imperative, then, to improve our alignment in the future. We have procured several alignment tools for this purpose, and both of these tests will be repeated.

Furthermore, because the tests cover two different regions, the systems have a slightly different focus. In order to make a comparison, therefore, it is necessary to select the region of comparison and to remove any focus term over that region. The region that has been selected for comparison is the radial zone between 70mm and 100mm.

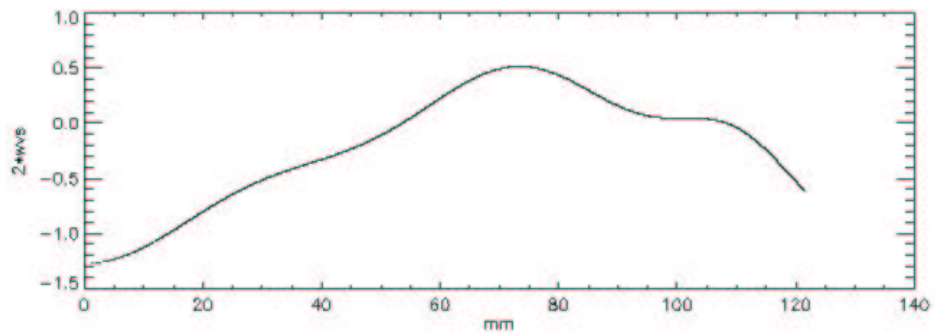
Figure 12 shows the scatter of $Z(\rho, \theta)$ overlaid for both tests. Figure 13 shows the average of these scatter plots over 0.1mm segments. The scatter of each line is approximately 0.02wvs RMS and the agreement between the two averaged scatter plots is 0.006wvs RMS.

4 Conclusion

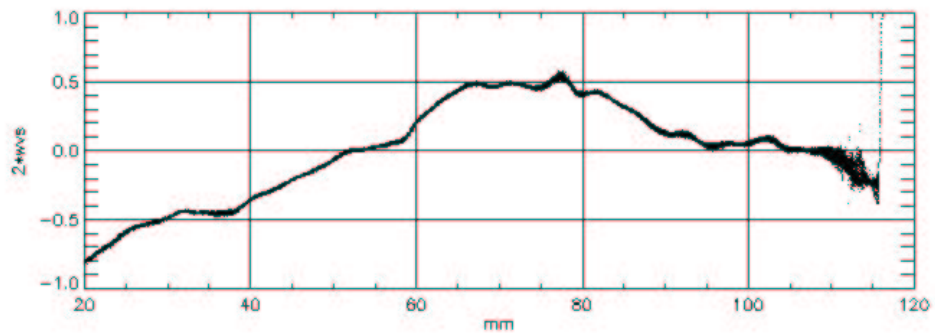
We have not received the mirror, yet significant progress has been made to qualify the optics involved in the Kodak mirror surface figure verification. The test plan involves many elements, both test optics and models. One of the most crucial optical elements is the CGH. The CGH must be verified, and to do so, it must be independently measured. A 9.5" parabolic mirror representing a sub-aperture of the Kodak mirror has been fabricated to do this verification. Its surface figure is measured with the CGH and also in double pass. Currently, the problem of extrapolating this agreement to the edge of the CGH remains. However, we have generated several concepts to deal with this source of uncertainty. Meanwhile, the largest hurdle in the qualification of the inner 9.5" of the CGH is the alignment of our test setups. Several pieces of hardware have been procured for the purpose of refining our setup. Despite this, the initial result is that the root summed squared error in the test optics (CGH and Transmission Sphere) is less than 0.008wvs RMS at spatial frequencies between 1.5mm and 30mm over the radial region 70mm-100mm. However, the actual test optic error is most likely less because the limit on the error reflects the uncertainty of the alignment of our test setups. Once the alignment of the test setups is improved, it is likely that the root sum square error in our test optics will be less than 0.005wvs or $\lambda/200$ – allowing a successful verification of the Kodak lightweight UV mirror.



(a)



(b)



(c)

Figure 8: *Top to Bottom:* (a) Radial projection of residual, (b) Spherical aberration terms from 2-D Zernike Fit, and (c) Total radial scatter.

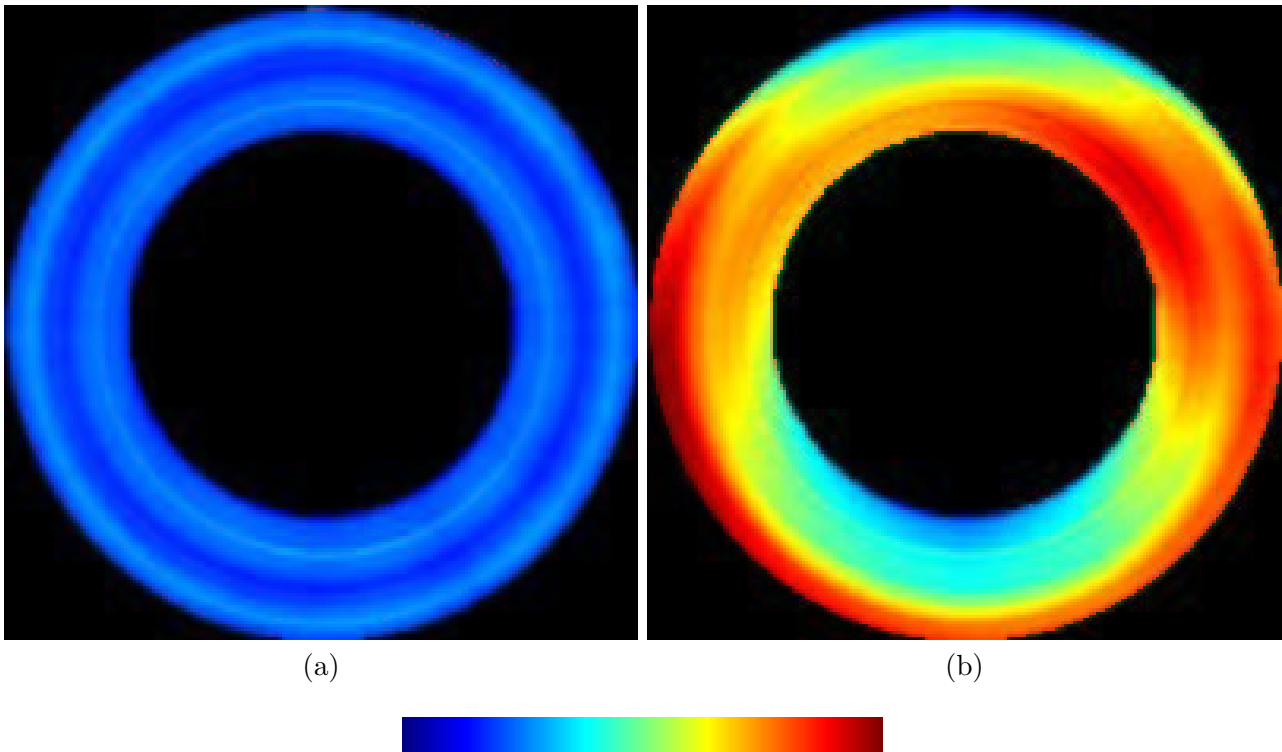


Figure 9: *Left to Right:* (a) Measured phase and (b) Extracted radial portion of the the sub-aperture parabola for the CGH test. The scale, at bottom, runs from 0wvs (at 632.8nm) to 0.8wvs.

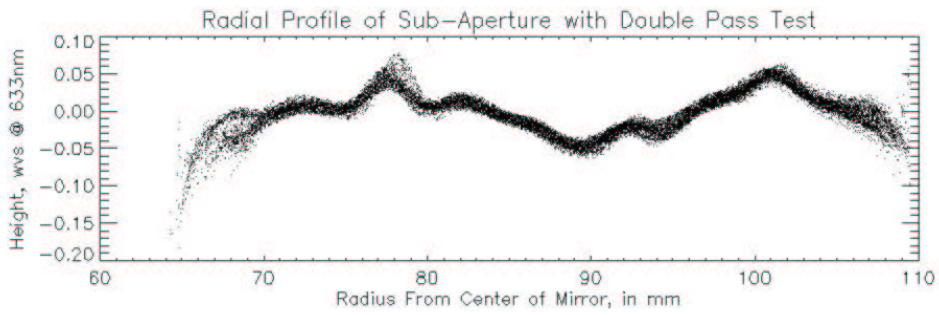


Figure 10: Radial profile of CGH error with low-order asymmetric Zernike terms removed.

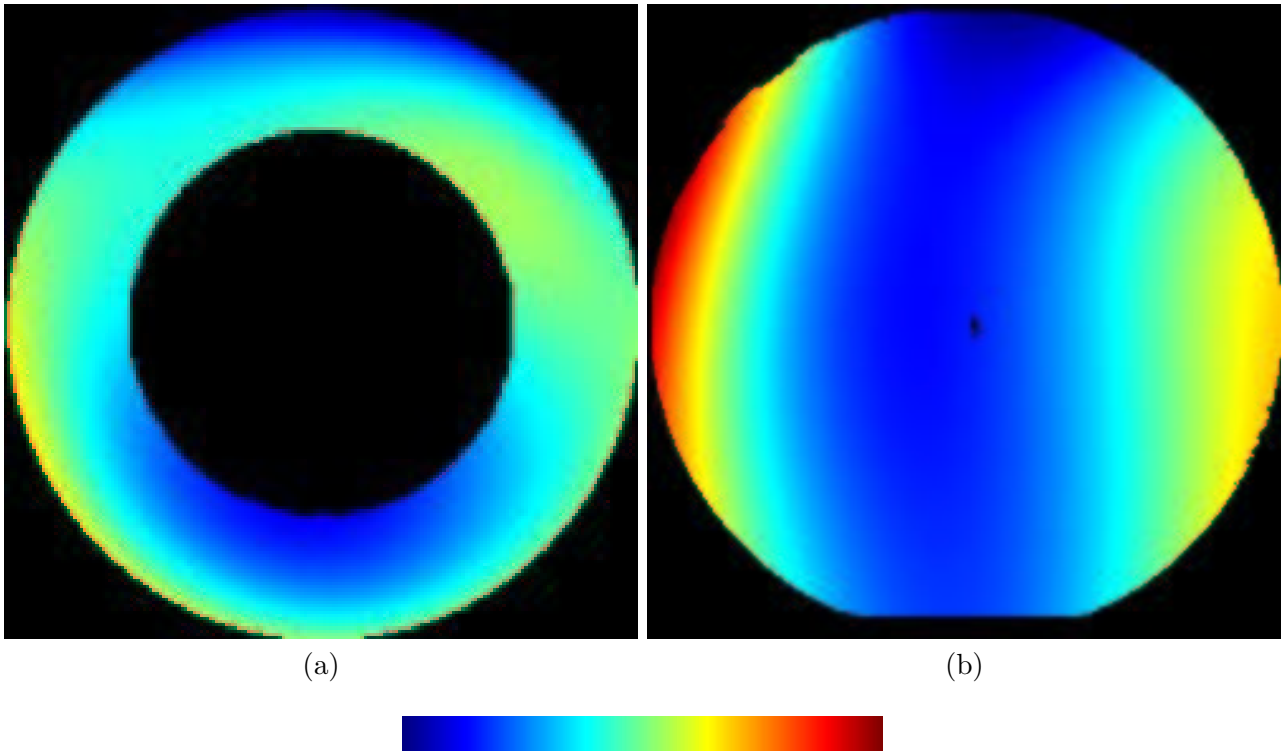


Figure 11: *Left to Right:* θ -dependent error removed from the: (a) CGH test (b) double-pass test. The scale, at bottom, runs from 0wvs (at 632.8nm) to 1.2wvs.

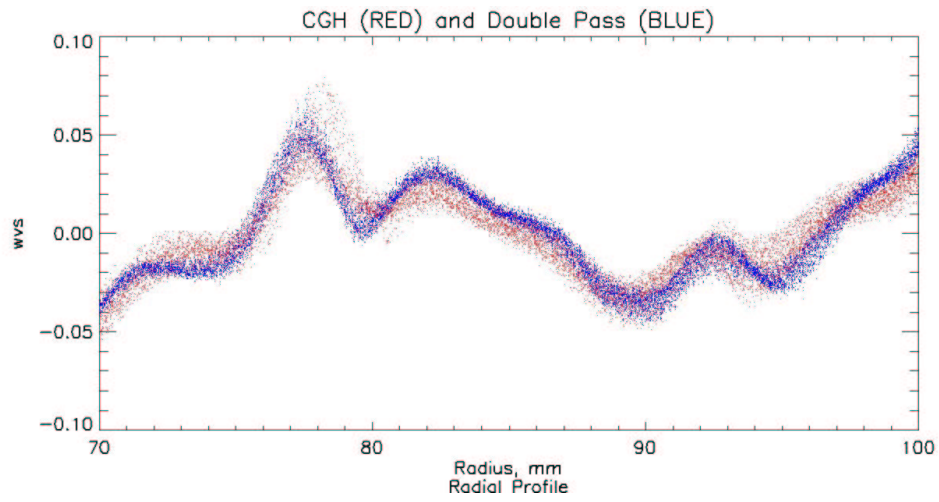


Figure 12: Scatter plots ($Z(\rho, \theta)$) for both the CGH and double-pass tests.

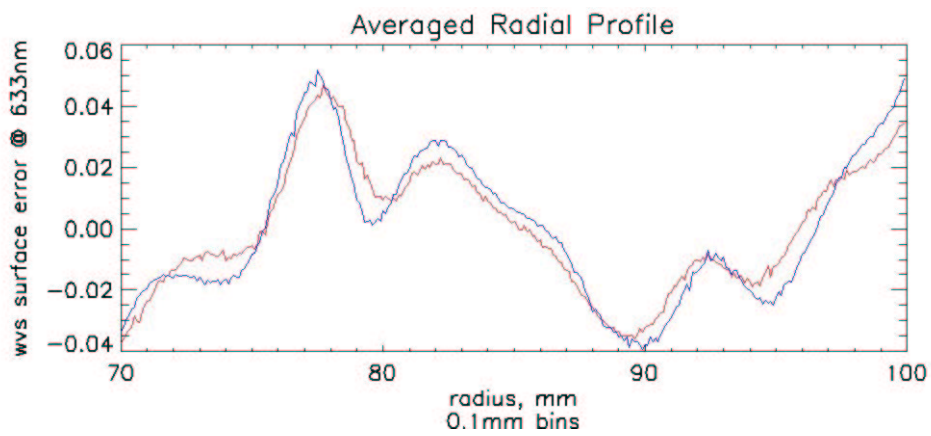


Figure 13: Radial profiles binned over 0.1mm segments.

Absolute Sphere Testing, Concept

